Optical Engineering

SPIEDigitalLibrary.org/oe

Study on spectral broadband aberration-corrected imaging spectrometer for far-ultraviolet waveband

Lei Yu
Shurong Wang
Yi Qu
Guanyu Lin

Study on spectral broadband aberration-corrected imaging spectrometer for far-ultraviolet waveband

Lei Yu
Shurong Wang
Yi Qu
Guanyu Lin
Changchun Institute of Optics
Fine Mechanics and Physics
Chinese Academy of Sciences
Changchun, Jilin 130033, China
E-mail: top1gods@mail.ustc.edu.cn

Abstract. In order for the Czerny–Turner spectrometer to be utilized in the imaging spectrometer for far-ultraviolet waveband, we describe the elimination of the principal aberration coma and astigmatism for the arrangement by light-path function analysis. The modified structure is built by a spherical mirror, a toroidal mirror, and a fixed plane grating. Starting with coma and astigmatism corrected by adjusting the incident angle to the collimating mirror and using a toroidal mirror, we obtain the optimized distances between the grating to the focusing mirror and the focusing mirror to the image plane by geometric analysis and first order differential calculation, in order to acquire high imaging quality in broad waveband. The design result shows a simple optical imaging structure that can be used in the ionosphere detection (120 to 180 nm) that is superior and convenient. [DOI: 10.1117/1.3591947]

Subject terms: aberrations; optical design; remote sensing; far ultraviolet; imaging spectrometer.

Paper 100850RRRR received Oct. 18, 2010; revised manuscript received Apr. 12, 2011; accepted for publication Apr. 27, 2011; published online Jun. 2, 2011.

1 Introduction

At present, different instruments detecting the ionosphere such as Atmospheric Infrared Sounder (AIRS), Global Ultraviolet Imager (GUVI), Special Sensor Ultraviolet Limb Imager (SSULI), and Ionospheric Mapping and Geocoronal Experiment (IMAGER),[1–4] have common characteristics: 1. These imaging spectrometers are basically formed by reflecting systems (e.g., AIRS: Elbert-Fastie, GUVI: Wadsworth structure with a toroidal grating, IMAGER: Gregorian telescope). 2. The optical structure is simple. Because signals of the ionosphere are very weak, the transmission energy achieved with detectors is very low in the far-ultraviolet waveband. Higher transmission efficiency can be guaranteed by fewer mirrors. 3. For the limit of the structure and the transmission energy, the image quality is poor for the structure that can be simply fabricated and aligned, and the optical structure that can obtain high image quality needs more advanced processing technology. For example, GUVI used toroidal grating and IMAGER used two nonspherical mirrors. An easier method with the ability to improve the disadvantages is required.

The Czerny–Turner spectrometer is one of the most frequently used instruments of resolving the spectral intensity of radiation imaged across one spatial dimension. The classic Czerny–Turner spectrometer consists of two spherical mirrors and one plane grating in symmetrical design.[5] Its performances are significantly influenced by geometrical aberration, especially coma generated by the off-axis reflection at the camera mirror and astigmatism due to different focal lengths in the meridian and sagittal planes. For disadvantages, the classic Czerny–Turner spectrometer does not have better image quality than a spectral broadband does in two spatial dimensions, so it is rarely used as an imaging spectrometer in remote sensing.

0091-3286/2011/$25.00 © 2011 SPIE

Most instruments using the Czerny–Turner structure take different techniques to eliminate influence caused by aberrations depending on wavelengths. The techniques include a scanned grating covering the entire spectral range, a CCD technology compensating moving parts aberration, and so on. But in spectroscopic imaging detection such as ionosphere/thermosphere, the corrections above are not enough. So the spectral region being suitable for imaging is limited for the positions of the grating of the spectrometer.

Many other proposals to improve the imaging performance of the Czerny–Turner spectrometer have been applied. A concave cylindrical grating was used instead of the plane grating by Dalton.[6] Nonspherical mirrors such as off-axis parabolic mirrors are used to reduce the distance between the entrance slit and the collimating mirror.[7] Toroidal focusing mirrors are accepted for their characteristics in reducing the astigmatism.[8] However, the common ground of these modifications is that these systems are mainly used for a monochrometer, which simultaneously examine a limited waveband or spectral lines one by one with a scanning structure. In Li Xu's recent work,[9] the design of freeform mirrors is used to make the Czerny–Turner spectrometer work effectively in a spectral broadband without moving grating. In Austin's work,[10] the divergent illumination method was introduced to make astigmatism free. The disadvantage of the divergent illumination method is that it did not consider the influence of coma. When the grating is put in the divergent illumination and the focusing mirror in spherical form, it will limit the *F*/# number of the system and reduce the imaging quality.

In this paper, a design of an optical system for far-ultraviolet imaging spectrometer is proposed to suppress aberrations. The system consists of two parts: the telescope objective is an off-axis parabolic mirror and the spectrum imaging system is a Czerny–Turner spectrometer. The main aberrations of coma and astigmatism are significantly corrected as discussed in Sec. 2. This design evidently increases

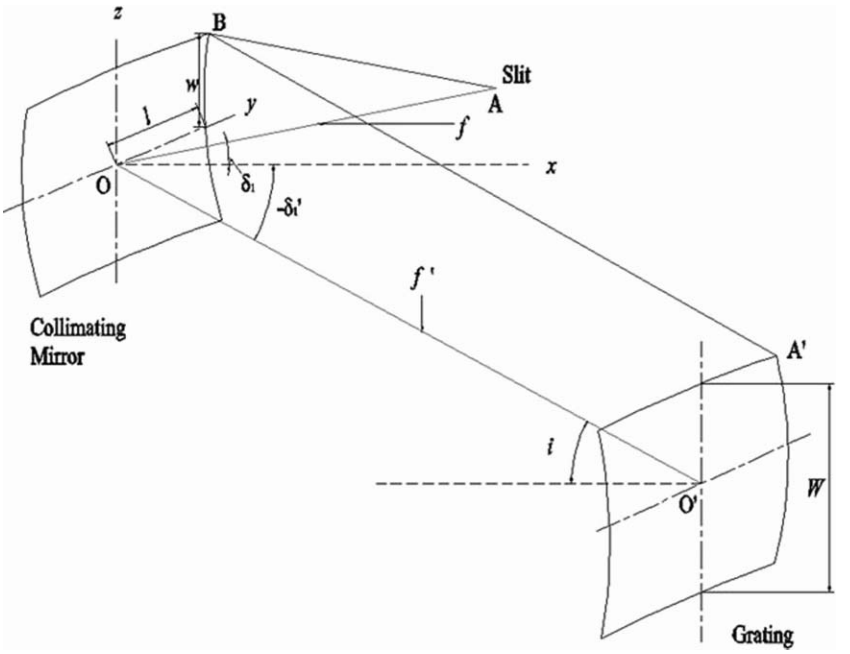

Fig. 1 Explanation for light-path function for collimating mirror and grating.

the spatial resolution and decreases RMS radius in X and Y directions in all wavebands without much energy loss.

2 Calculation and Correction Methods of the Aberrations

2.1 *Elimination of Coma and Astigmatism*

By following and extending Shafer and Beutler's theory,[11] the extending light-path function of the collimating mirror and the plane grating using two parameters w and l in two dimensions is obtained. This extends Shafer and Beutler's theory in which only w was used

$$F = F_{00} + F_{10} + F_{20} + F_{30} + F_{02} + F_{12}.... \tag{1}$$

The items are as follows: $F_{00} = f + f'$ is a constant; for $\delta_1 = -\delta_1'$, $F_{10} = w(\sin\delta_1 + \sin(-\delta_1')) = 0$;

$$F_{20} = \frac{w^2}{2}\left(\frac{\cos^2\delta_1}{f} - \frac{2\cos\delta_1}{R_{1M}} + \frac{\cos^2\delta_1}{f'}\right);$$

$$F_{30} = \frac{w^3}{2}\left[\frac{\sin\delta_1}{f}\left(\frac{\cos^2\delta_1}{f} - \frac{\cos\delta_1}{R_{1M}}\right) - \frac{\sin\delta_1}{f'}\left(\frac{\cos^2\delta_1}{f'} - \frac{\cos\delta_1}{R_{1M}}\right)\right];$$

$$F_{02} = \frac{l^2}{2}\left(\frac{1}{f} - \frac{2\cos\delta_1}{R_{1S}} + \frac{1}{f'}\right);$$

and

$$F_{12} = \frac{wl^2}{2}\left[\frac{\sin i}{f}\left(\frac{1}{f} - \frac{\cos i}{R_{1S}}\right) + \frac{\sin\theta}{f'}\left(\frac{1}{f'} - \frac{\cos\theta}{R_{1S}}\right)\right].$$

F_{20} and F_{02} are corresponding with astigmatism. F_{30} and F_{12} are corresponding with coma. In Fig. 1, the direction of the slit (slit length) is perpendicular to the meridian plane xOz, which is also the symmetry plane of the optical system. The symbols are explained in Fig. 1. δ_1 and δ_2 are the incident angles of the collimating and focusing mirrors. R_{1M} and R_{2M} are the radii of the two mirrors in the meridian direction. R_{1S} and R_{2S} are the radii of the two mirrors in the sagittal direction. W is the projected width of the grating upon the collimating mirror. θ and i are determined by the geometric configuration for the grating as

$$d(\sin i + \sin\theta) = m\lambda. \tag{2}$$

Because the length of the slit in the sagittal direction is much longer than in the meridian direction, the image will extend to several millimeters along the slit due to the astigmatism brought by different focal lengths of the mirrors in two directions.[8]

For the collimating mirror, if we want the astigmatism in the meridian direction to be corrected, F_{20} will be zero. Applying Fermat's principle with $f' = 0$ to indicate a plane wave, we get

$$F_{20}(f' = 0) = \frac{w^2}{2}\left(\frac{1}{f} - \frac{2}{R_{1M}\cos\delta_1}\right) = 0. \tag{3}$$

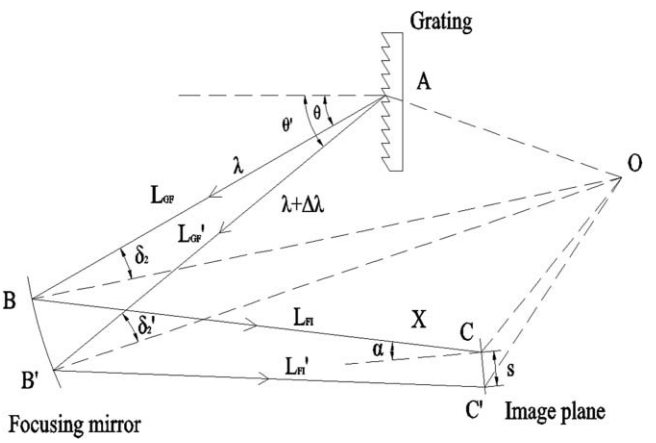

Fig. 2 Showing the central wavelength λ and another with a slightly different △λ wavelength, whose displacement on the image plane is *s*.

Table 1 Particles parameters intensities.

Particles	Day intensities		Night intensities		Auroral intensities	
Wavelength/nm	Max(R)	Min(R)	Max(R)	Min(R)	Max(R)	Min(R)
H^+:121.6	30000	2000	10000	500	5000	500
$O\vert$:130.4	20000	1000	300	20	20000	100
$O\Vert$:135.6	4000	50	200	15	4000	50
N_2:140–150	1000	15	n/a	n/a	3000	50
N_2:165–180	500	120	n/a	n/a	2000	400

So,

$$f = f_{1M} = \frac{R_{1M}\cos\delta_1}{2}. \tag{4}$$

The similar calculation can also be used for the focusing mirror and image plane. We have

$$f' = f_{2M} = \frac{R_{2M}\cos\delta_2}{2}. \tag{5}$$

By the same principle that F_{02} is zero, we calculate f_{1S} and f_{2S} for the sagittal direction as

$$f_{1S} = \frac{R_{1S}}{2\cos\delta_1} \tag{6}$$

and

$$f_{2S} = \frac{R_{2S}}{2\cos\delta_2}. \tag{7}$$

When

$$\begin{aligned}\Delta f_{\text{overall}} &= (f_{1S} - f_{1M}) + (f_{2S} - f_{2M}) \\ &= \left(\frac{R_{1S}}{2\cos\delta_1} - \frac{R_{1M}\cos\delta_1}{2}\right) + \left(\frac{R_{2S}}{2\cos\delta_2} - \frac{R_{2M}\cos\delta_2}{2}\right) = 0,\end{aligned} \tag{8}$$

Table 2 Specification of designed imaging spectrometer.

Spectral coverage/nm	120 to 180
Instrument FOV/(°)	4×0.1
Detector pixel size/μm	24×24
Focal length/mm	111.4
F/#	6.6
Target spatial coverage /km	Limb 50–520
Spatial resolution (Limb/Nadir) /km	1/0.6
Spectral resolution /nm	1.5 to 2.5

Table 3 Parameters of optical structure.

Characteristic	Orginal	ZEMAX
Entrance aperture		
Clear aperture	Φ16 mm	Φ16 mm
Telescope mirror		
Type	Off-axis parabola	
Off-axis distance	15 mm	15 mm
Focal length	100 mm	100 mm
Entrance slit		
Size	0.25 mm×7.1 mm	0.25 mm×7.1 mm
Angular resolution	0.1 deg ×4 deg	0.1 deg ×4 deg
Collimating mirror		
Type	sphere	
Incident angle δ_1	9.5502 deg	9.7508 deg
Curvature, r_1^b(S,T)	250 mm, 250 mm	250 mm, 250 mm
Grating		
Type	plane	plane
Ruling	600 Grooves/mm	600 Grooves/mm
Incident angle	10.37 deg	10.37 deg
Diffraction angle	4.58 deg	4.58 deg
Condensing mirror		
Type	Toroidal	
Incident angle δ_2	12.1734 deg	11.3847 deg
Curvature, r_2^b(T,S)	277.185 mm, 260 mm	278.646 mm, 260 mm
Distance L_{GF}	250 mm	250 mm
Image plane		
Inclined angle α	20 deg	20 deg
Distance L_{GI}	134.6 mm	135.6 mm

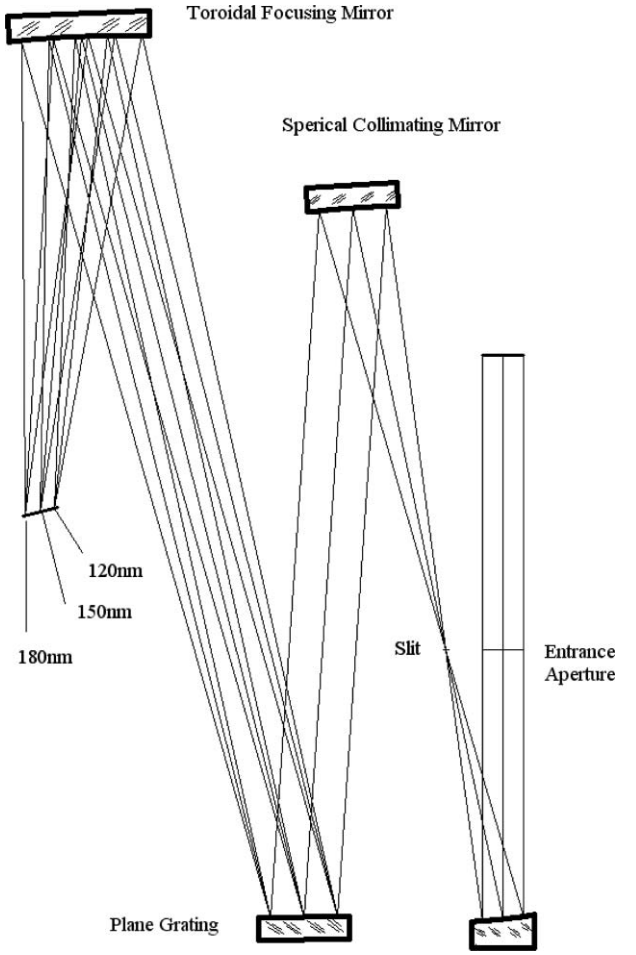

Fig. 3 Design of imaging spectrometer optical system.

the astigmatism introduced by the adding focal length $\triangle f_{\text{overall}}$ will be corrected. In the advanced design, the collimating mirror is a spherical mirror that makes $f_{1S} - f_{1M} > 0$. And the focusing mirror is in toroidal form of which the radius in the meridian direction is longer than in the sagittal direction to make $f_{2S} - f_{2M} < 0$ and $(f_{1S} - f_{1M}) \approx (f_{2S} - f_{2M})$. We can adjust the radii in two directions of the focusing mirror to make $\triangle f_{\text{overall}}$ zero.

The light-path function for a mirror has also been used to calculate coma. It should be known that when the astigmatism is corrected, F_{12} is also zero for the choices of f_{iM} and f_{iS}. Then the residual coma is only corresponding with w. And the problem degrades into an identical one as with Shafer's.[11] So the coma eliminated condition is as follows:

$$\frac{\sin\delta_1}{\sin\delta_2} = \left(\frac{R_{1M}}{R_{2M}}\right)^2 \left(\frac{\cos\theta\cos\delta_1}{\cos i\cos\delta_2}\right)^3 = \left(\frac{R_{1M}}{R_{2M}}\right)^2 \left(\frac{\cos\theta}{\cos i}\right)^3. \tag{9}$$

In general, δ_1 and δ_2 are as small as possible. So, $\cos^3\delta_1$ and $\cos^3\delta_2$ are about 1. Thus, the condition can be met by optimizing the incident angle to the collimating mirror with the fixed focusing mirror and setting R_{2M} larger than R_{1M}. It should be known that the optimal astigmatism correction obtained depends on different incidence angles to the focusing mirror for different radii. Moreover, the incidence angle is related to the diffraction angle of the grating. The coma elimination condition is first obtained by Shafer et al., and the condition is commonly used and effectively proven in later designs and literatures.

2.2 *Correction Formulas under First-order Condition in Spectral Broadband*

In order to obtain the condition that the spectrometer maintains the same performances in all wavebands, the geometric method and the first-order differential condition are introduced.

As shown in Fig. 2, we construct a two-dimensional vectors coordinate system. Then we can get several vector triangles: ABO, $AB'O$, OBC, $OB'C'$, and OCC', and obtain the equations

$$\begin{cases} \overrightarrow{OB} - \overrightarrow{AB} = \overrightarrow{OB'} - \overrightarrow{AB'} = \overrightarrow{OA} \\ \overrightarrow{OC'} - \overrightarrow{OC} = (\overrightarrow{OB'} - \overrightarrow{C'B'}) - (\overrightarrow{OB} - \overrightarrow{CB}) = \overrightarrow{CC'} \end{cases}. \tag{10}$$

For the geometric relationship, we can get such pairs of equations in two directions

$$\begin{cases} L_{GF}\cos\theta - R_{2M}\cos(\theta - \delta_2) = L'_{GF}\cos\theta' - R_{2M}\cos(\theta' - \delta'_2) \\ L_{GF}\sin\theta - R_{2M}\sin(\theta - \delta_2) = L_{GF}\sin\theta' - R_{2M}\sin(\theta' - \delta'_2) \end{cases} \tag{11}$$

and

$$\begin{cases} R_{2M}\cos(\theta - \delta_2) - R_{2M}\cos(\theta' - \delta'_2) + L'_{FI}\cos(2\delta'_2 - \theta') - L_{FI}\cos(2\delta_2 - \theta) = s\sin(\alpha - 2\delta_2 + \theta) \\ R_{2M}\sin(\theta - \delta_2) - R_{2M}\sin(\theta' - \delta'_2) + L'_{FI}\sin(2\delta'_2 - \theta') - L_{FI}\sin(2\delta_2 - \theta) = s\cos(\alpha - 2\delta_2 + \theta) \end{cases}. \tag{12}$$

L_{GF} and $L_{GF'}$ are the distances between the grating and the focusing mirror, L_{FI} and $L_{FI'}$ are the distances between the focusing mirror and the image plane, α is the focusing mirror with the angle of incidence in the tangential plane, and s is the width of the image plane. Here, we know that the optimal incident angle relies on incident and diffraction angles of the grating. Therefore, if different incidence angles to the focusing mirror are identical, the aberrations for

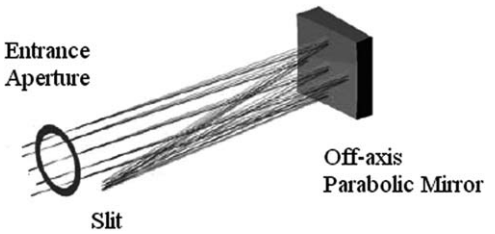

Fig. 4 Structure of the telescope.

different wavelengths will be simultaneously corrected by the same optical parameters. It occurs when the grating is in the collimating illumination, which leads the incident angle δ_2 and distance L_{FI} to have no relationships with the diffracted angle θ of the grating. It can be expressed with the above equations' differential calculations. We differentiate Eqs. (11) and (12) with respect to θ and obtain the resulting expressions (13) and (14) for the optimal distances

$$\begin{cases} \dfrac{d\delta_2}{d\theta} = 1 - \dfrac{L_{GF}}{R_{2M}\cos\delta_2} = 0 \\ \dfrac{dL_{FI}}{d\theta} = \tan\alpha\left(L_{GF} + L_{FI} - \dfrac{2L_{GF}L_{FI}}{R_{2M}\cos\delta_2}\right) - L_{GF}\tan\delta_2 = 0 \end{cases}. \tag{13}$$

So,

$$\begin{cases} L_{GF} = R_{2M}\cos\delta_2 \\ L_{FI} = R_{2M}\cos\delta_2\left(1 - \dfrac{\tan\delta_2}{\tan\alpha}\right) \end{cases}. \tag{14}$$

In the work of Xue et al.,[12] the similar result [first formula in Eq. (14)] is obtained, and Austin et al.[10] also proposed similar derivations. He used the grating under the zeroth-order divergent illumination condition to eliminate the astigmatism. The advantage of his method is that the focusing mirror can be chosen as a spherical mirror but the disadvantage of it is that coma is neglected. So for his method, we cannot use the same criterion and cannot obtain the identical optimal conditions as Eq. (14). Our similar derivations are based on the fact that the grating is under the collimating illumination and the focusing mirror is a toroidal mirror, of which astigmatism correction does not depend on wavelengths. It eliminates coma in advance and makes the $F/\#$ number of the system smaller. So the energy that the optical system accepted is larger and the imaging quality is better. It is especially important for the spectrometer used in weak signal detection such as ionosphere detection. Also with the different principle, the first and second formulas in Eq. (14) that have not been presented were proposed. It will be proven in the following example.

3 Application to the Design of an Imaging Spectrometer Working in 120 to 180 nm

3.1 *Environmental and Design Parameters*

It assumes that the system works in the orbit of 833 km. The operation modes include limb and nadir viewing. In the limb mode, the spectrometer view a tangent point from 50 to 520 km above the horizon, at a distance of 3267.9 to 2166 km. The particles to be detected are shown in Table 1. The basic specifications of the spectrometer are shown in Table 2.

The optical parameters of calculation results of previous sections and optimization by ray tracing[13] with the help of ZEMAX are listed in Table 3.

The optical system of the imaging spectrometer is shown in Fig. 3.

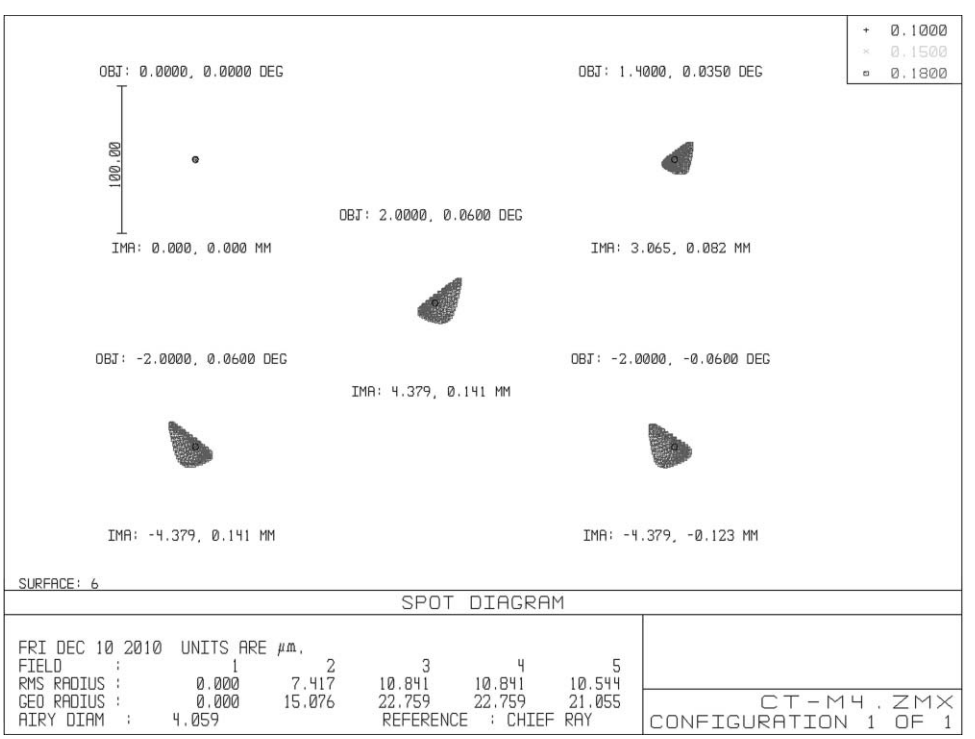

Fig. 5 Image RMS spot diagrams at the entrance slit.

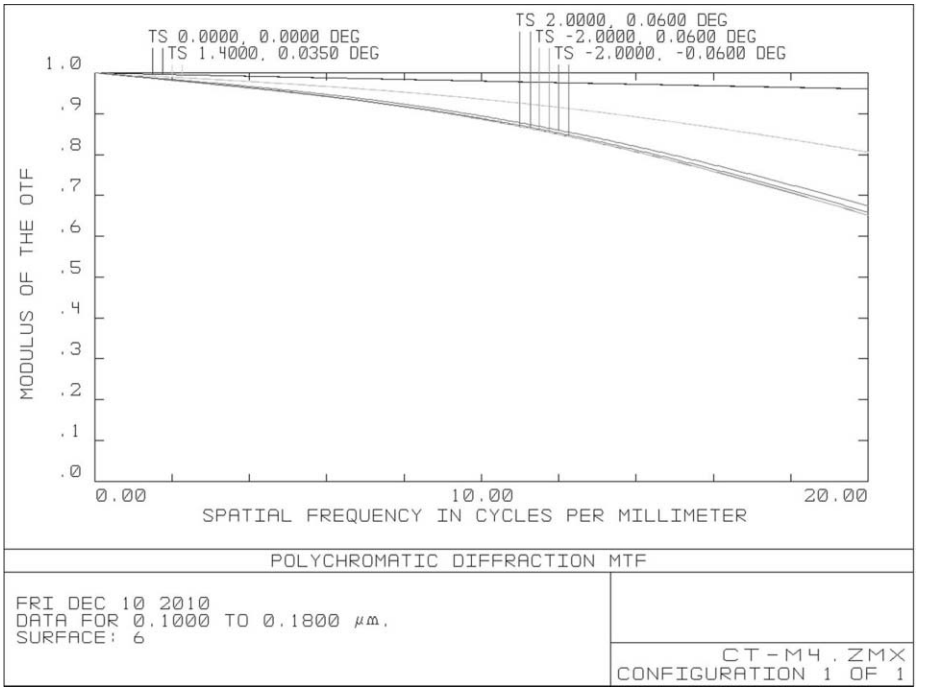

Fig. 6 MTF of the telescope at the entrance slit in wavelengths.

3.2 *Ray Tracing Analysis*

The telescope of the spectrometer is shown in Fig. 4.

The off-axis parabolic mirror can eliminate aberration on the axis, but the aberration will be larger with the increase of the off-axis distance and angle. The appropriate choices of the distance and angle can decrease the off-axis aberration. We used ZEMAX to design and optimize the telescope. The stop is on the focal plane of the telescope, and it is a telecentric object light path. The image RMS spot radius generated at the slit by the parabolic telescope mirror is shown in Fig. 5. The MTF of the telescope is shown in Fig. 6. It shows that the diameters of the spots are smaller than 23 μm and the MTF is larger than 0.6 at the frequency 20 lp/mm.

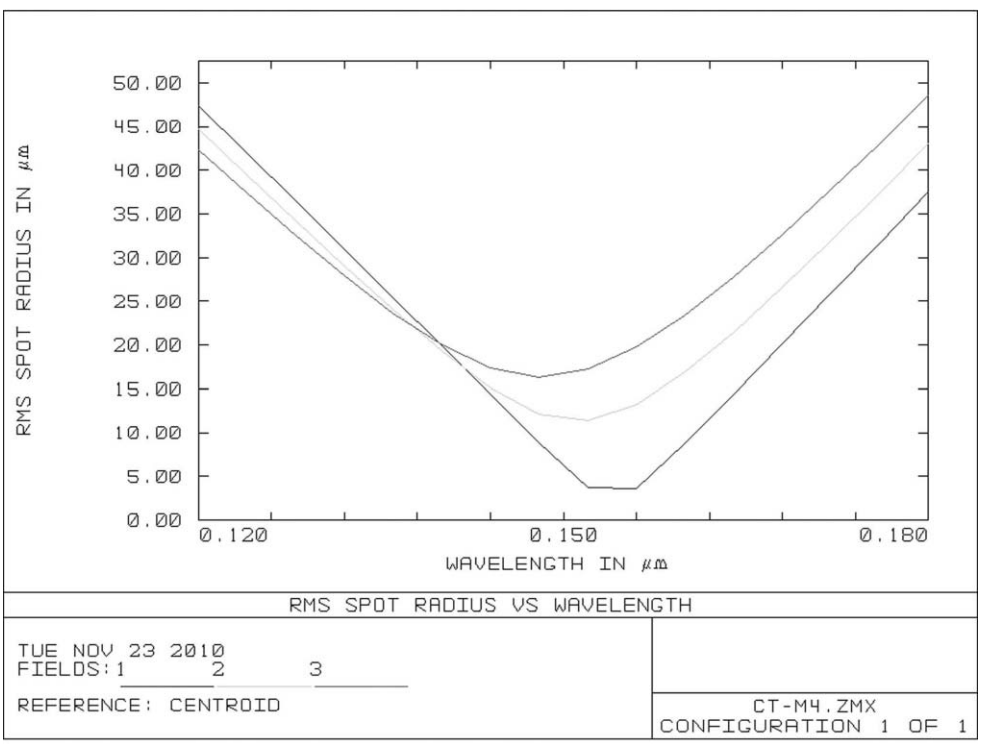

Fig. 7 RMS spot radius versus wavelength for $L_{GF} = R_2\cos\delta_2/2$.

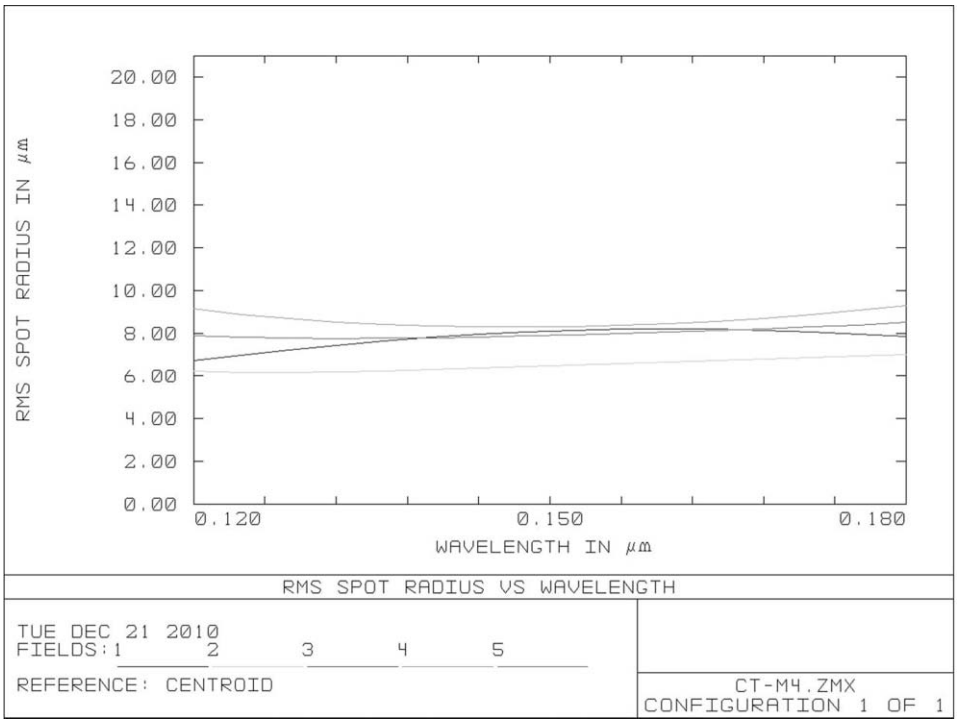

Fig. 8 RMS spot radius versus wavelength for $L_{GF} = R_2\cos\delta_2$, $L_{FI} \neq R_2\cos\delta_2(1 - \tan\delta_2/\tan\alpha)$, and torodial focusing mirror.

To show advantages of the corrected Czerny–Turner system, different design results are expressed in Figs. 7–9. In Fig. 7, the best image quality of the existing arrangement ($L_{GF} = R_2\cos\delta_2/2$ and the focusing mirror is a spherical mirror) appears only in the vicinity of the waveband. But in Fig. 8, good image quality of the advanced arrangement [$L_{GF} = R_2\cos\delta_2$, $L_{\mathrm{FI}} = R_2\cos\delta_2(1 - \tan\delta_2/\tan\alpha)$ and the focusing mirror is a torodial mirror] is obtained over the whole waveband. The RMS geometric spot radii in two directions did not exceed 10 μm in all of the wavebands.

To make the spectrum incident on the image plane uniform, no defocus and curve the condition L_{FI}

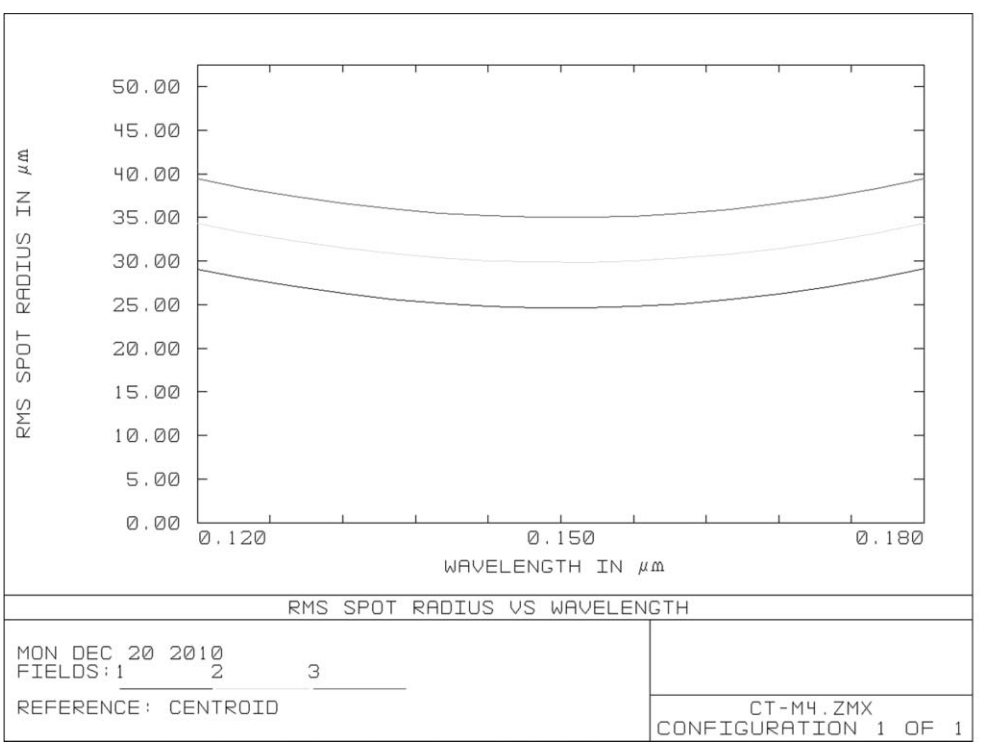

Fig. 9 RMS spot radius versus wavelength for $L_{FI} \neq R_2\cos\delta_2(1 - \tan\delta_2/\tan\alpha)$.

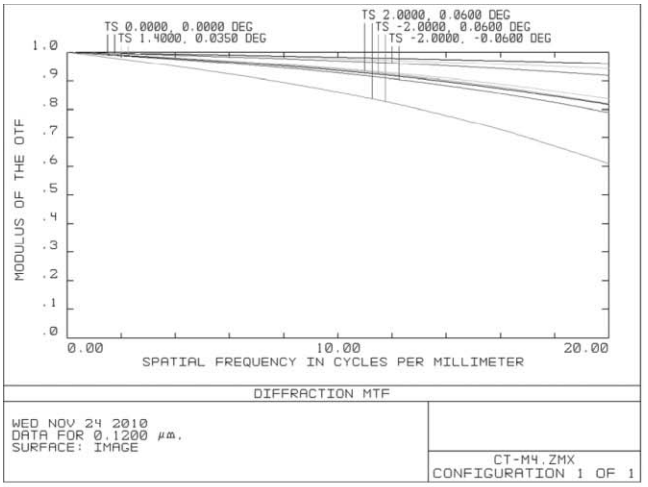

(a)

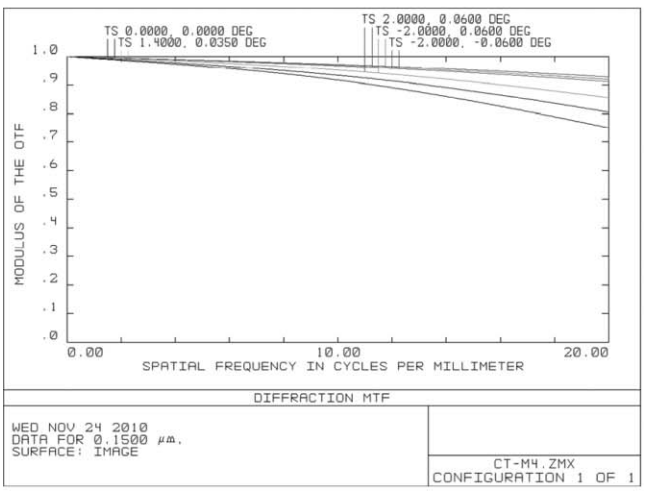

(b)

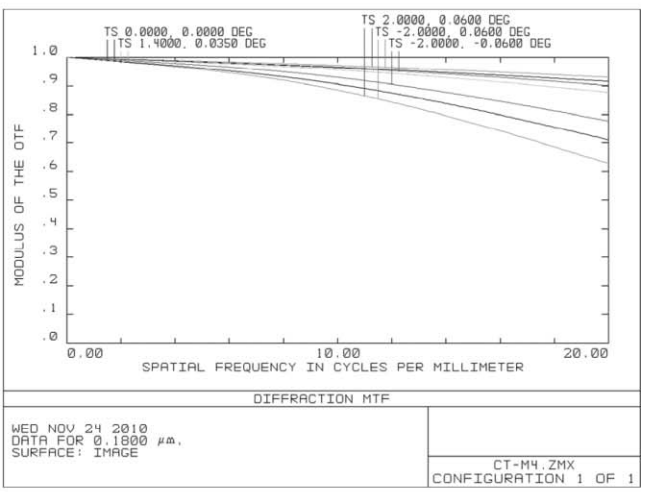

(c)

Fig. 10 MTF of the FUV imaging optical system in the central and marginal wavelengths. Data for (a) 0.1200 μm, (b) 0.1500 μm, and (c) 0.1800 μm.

$= R_{2T}\cos\delta_2(1-\tan\delta_2/\tan\alpha)$ must be satisfied. Based on the optical parameters of the system, we calculate that the range of α is (19.2 deg, 22 deg). The range guarantee L_{FI} is near $R_{2T}/2$. To facilitate assembly of the image plane, the angle was chosen as 20 deg. Figure 9 shows the distance L_{FI}

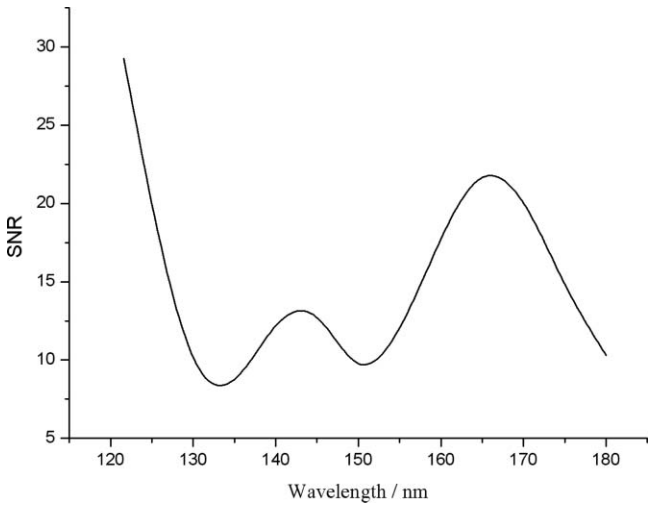

Fig. 11 SNRs of different wavelengths.

$\neq R_{2T}\cos\delta_2(1-\tan\delta_2/\tan\alpha)$ (134.6 mm) at 20 deg. From Figs. 8 and 9 we know that L_{FI} greatly influences results.

By final optimization, excellent image quality at the image plane is obtained. The modulation transfer function (MTF) curves are functions of spatial frequency. Figures 10(a)–10(c) present the values of MTF for central and marginal wavelengths. The different color curves stand for different field of views. It is clear that the MTF of each field is larger than 0.6 at the Nyquist frequency of the detector for central and marginal wavelengths.

3.3 *Signal-to-Noise Ratio Analysis*

The designed system includes three mirrors, which is as many as AIRS and more than the other loads such as GUVI (one mirror and one grating), RAIDS (two mirrors and one grating), and HITS (one mirror and one grating). But it does not mean that the ability of collecting signals of the system is much lower than the others. It is because the diffraction efficiency of the blazing plane grating is higher than the concave grating. The diffraction efficiency of the blazing plane grating is nearly 40%, but only about 30–35% for concave grating in FUV. With the assumed condition that the reflection efficiency of mirrors is 80%, the transmission efficiency of GUVI is 24%, RAIDS is 22%, and the designed system is 20%. It can be seen that the differences of transmission efficiencies between the design and the other loads are not large.

The signal-to-noise ratio for the system can be expressed by[14]

$$SNR = S/\sqrt{S + n_{dark} + \sigma_{read}^2}, \tag{15}$$

where n_{dark} is the dark current noise and σ_{read} is the readout noise. They are decided by the detector and the electric circuit. For the chosen delay-line detector, n_{dark} and σ_{read} are much smaller than S. S is the signal arriving at the detector, which can be calculated by

$$S = \frac{\pi}{8F^2hc}\tau(\lambda)\eta(\lambda)A_s t_{\text{int}} R, \tag{16}$$

where F is the F number, $h = 6.63 \times 10^{-34}$ m^2 kg/s, $c = 3 \times 10^8$ m/s^2, $\tau(\lambda)$ is the transmission efficiency, $\eta(\lambda)$ is the quantum efficiency of the detector surface, A_s is the area of the

detector, t_{int} is the integration time, and R is the wavelengths spectral intensities whose unit is Rayleigh. Then we can calculate SNR of the designed system and get Fig. 11.

The SNRs are all larger than five. It proves that the designed system is available.

4 Summary and Conclusion

A design using the Czerny–Turner spectrometer is suggested for the 120 to 180 nm imaging spectrometer. It is feasible to suppress aberration with simple fabrication and alignment in the instrument. The light-path function is used to analyze coma and astigmatism. A torodial focusing mirror can solve the problem. The geometric vector method and the first-order differential calculation supplied the two correct distances between the grating and focusing mirrors, and the focusing mirror to the image plane. The technique compensates astigmatism in the spectrum broadband without complicating the mirror surfaces. The ray-tracing result has shown that RMS spot Y sizes were reduced to about 20 μm without increasing RMS spot X sizes in 120 to 180 nm. The analysis of SNR indicates that the designed system is available. So the structure is suited for using applications in space remote sensing imaging, especially in ionosphere exploration.

Acknowledgments

Research was supported by the National Natural Science Foundation of China (NSFC) under Grant No. 41074126.

References

1. F. W. Schenkel, B. S. Ogorzalek, J. C. Larrabee, F. J. LeBlanc, and R. E. Huffman, "Ultraviolet daytime auroral and ionospheric imaging," *Appl. Opt.* **24**, 3395–3405 (1985).
2. L. J. Paxton, A. B. Christensen, D. Morrison, B. Wolven, H. Kil, Y. Zhang, B. S. Ogorzalek, D. C. Humm, J. Goldsten, R. DeMajistre, and C. I. Meng, "GUVI: a hyperspectral imager for geospace," *Proc. SPIE* **5660**, 228–239 (2004).
3. R. P. McCoy, K. F. Dymond, G. G. Fritz, S. E. Thonnard, R. R. Meler, and P. A. Regeon, "Special sensor ultraviolet limb imager: an ionospheric and neutral density profiler for the Defense Meteorological Satellite Program satellites," *Opt. Eng.* **33**, 423–429 (1994).
4. P. C. Kalmanson, J. Wilczynski, K. Wood, K. Dymond, S. Thonnard, and J. Spann, "The optomechanical design and operation of the ionospheric mapping and geocoronal experiment," *Proc. SPIE* **5901**, 59010Q-1–59010Q-14 (2005).
5. M. Czerny and A. Turner, "Über den Astigmatismus Speigelspektrometern," *Z. Phys. A* **61**, 792–797 (1930).
6. M. L. Dalton, Jr., "Astigmatism compensation in the Czerny-Turner spectrometer," *Appl. Opt.* **5**, 1121–1123 (1966).
7. B. Bates, M. McDowell, and A. C. Newton, "Correction of astigmatism in a Czerny-Turner spectrograph using a plane grating in divergent illumination," *J. Phys. E* **3**, 206–210 (1970).
8. M. Futamata, T. Takenouchi, and K.-I. Katakura, "Highly efficient and aberration-corrected spectrometer for advanced Raman spectroscopy," *Appl. Opt.* **41**, 4655–4665 (2002).
9. L. Xu, K. Chen, Q. He, and G. Jin, "Design of freeform mirrors in Czerny-Turner spectrometers to suppress astigmatism," *Appl. Opt.* **48**, 2971–2879 (2009).
10. D. R. Austin, T. Witting, and I. A. Walmsley, "Broadband astigmatism-free Czerny-Turner imaging spectrometer using spherical mirrors," *Appl. Opt.* **48**, 3846–3853 (2009).
11. A. Shafer, L. R. Megill, and A. Droppleman, "Optimization of the Czerny-Turner spectrometer," *J. Opt. Soc. Am.* **54**, 879–887 (1964).
12. Q. Xue, S. Wang, and F. Lu, "Aberration-corrected Czerny-Turner imaging spectrometer with a wide spectral region," *Appl. Opt.* **48**(1), 11–16 (2009).
13. ZEMAX is a trademark of Zemax Development Corporation, Bellevue, Washington 98004, USA.
14. L. Yu, L. G.-Y. Lin, Y. Qu, and S.-R. Wang, "Analysis and experimental verification of SNR for a far ultraviolet imaging spectrograph in 115nm-180nm," *Spectrosc. Spectral Anal. (Beijing)* **30**(11), 3156–3160 (2010).

Biographies and photographs of the authors not available.